Modelling the viral dynamics of the SARS-CoV-2 Delta and Omicron variants in different cell types

Clare P. McCormack[1]*, Ada W. C. Yan[2]*, Jonathan C. Brown[2], Ksenia Sukhova[2], Thomas P. Peacock[2], Wendy S. Barclay[2], Ilaria Dorigatti[1]

[1]MRC Centre for Global Infectious Disease Analysis, School of Public Health, Imperial College London, London, United Kingdom

[2]Department of Infectious Disease, Imperial College London, London, United Kingdom

*contributed equally, joint corresponding authors

Abstract

We use viral kinetic models fitted to viral load data from *in vitro* studies to explain why the SARS-CoV-2 Omicron variant replicates faster than the Delta variant in nasal cells, but slower than Delta in lung cells, which could explain Omicron's higher transmission potential and lower severity. We find that in both nasal and lung cells, viral infectivity is higher for Omicron but the virus production rate is higher for Delta. However, the differences are unequal between cell types, and ultimately leads to the basic reproduction number and growth rate being higher for Omicron in nasal cells, and higher for Delta in lung cells. In nasal cells, Omicron alone can enter via a TMPRSS2-independent pathway, but it is primarily increased efficiency of TMPRSS2-dependent entry which accounts for Omicron's increased activity. This work paves the way for using within-host mathematical models to understand the transmission potential and severity of future variants.

Introduction

Since its designation as a variant of concern (VOC) by the World Health Organization on 26th November 2021[1], the Omicron (B.1.1.529\BA.1) variant of severe acute respiratory coronavirus 2 (SARS-CoV-2) has rapidly displaced the Delta (B.1.617.2) variant to become the dominant SARS-CoV-2 variant globally[2–4]. Analyses have demonstrated that Omicron can partially evade the immunity generated through previous infection and vaccination[5–8], thereby leading to reduced vaccine effectiveness against symptomatic disease[9].

Despite this reduction in vaccine effectiveness against symptomatic disease, the risk of severe outcomes (including hospital admission and death) following infection with Omicron is substantially lower than following infection with Delta, for both vaccinated and unvaccinated individuals[10,11]. While much remains to be understood about the mechanisms underpinning this observation, a reduction in the capacity of Omicron relative to Delta to replicate in lung cells has been suggested as a possible explanation[12]. On the other hand, Omicron's increased ability to replicate in nasal cells has been suggested as an explanation for Omicron's transmission advantage over Delta observed from epidemiological data[13–15].

It has been hypothesised that these differences in viral replication capacity in different cells can be attributed to how Omicron and Delta utilise different pathways to enter host cells[12,16–18]. All SARS-CoV-2 viruses can enter cells which express both ACE2 and TMPRSS2 proteins, via fusion of the viral and cell membranes or via early endosomes[19]. However, Omicron is also able to efficiently enter ACE2+ cells via fusion from the endosome after endocytosis, without the involvement of TMPRSS2[16,20]. This could expand the range of cells that Omicron can infect. A complication is by entering cells via the endosome, SARS-CoV-2 may be inhibited by endosomal restriction factors such as interferon-induced IFITM proteins[21,22] or NCOA7[23]. Understanding how virological properties shape the viral dynamics of SARS-CoV-2 in different cell types can enhance our understanding of the mechanisms underlying the observed differences in transmissibility between the Omicron and Delta variants. The different entry pathways and their inhibition by endosomal restriction factors are shown in Figure 1.
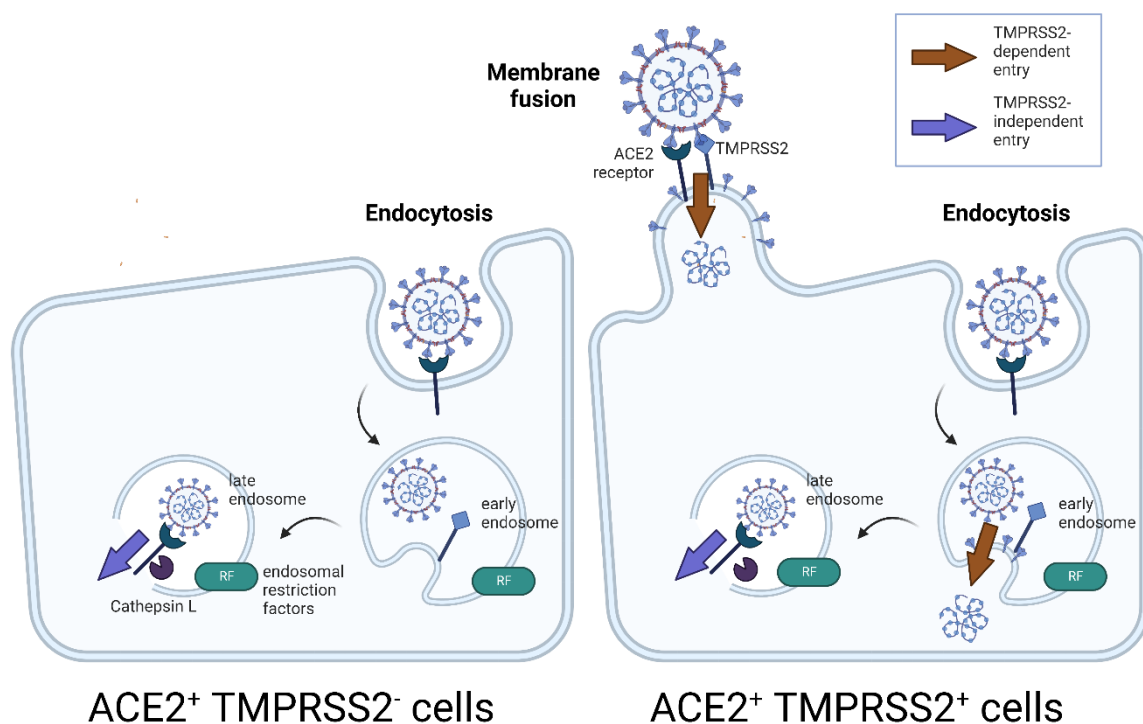
Figure 1. Illustration of TMPRSS2-dependent and TMPRSS2-independent entry pathways and their inhibition by endosomal restriction factors. In ACE2+ TMPRSS2+ cells (right), virus can enter in a TMPRSS2-dependent way via membrane fusion either at the cell surface or the early endosome; alternatively, virus can enter in a TMPRSS2-independent way through the late endosome. In ACE2+ TMPRSS2- cells (left), only the TMPRSS2-independent pathway is available. Both pathways can be inhibited by endosomal restriction factors. Created with BioRender.com.

Mechanistic mathematical models, calibrated against virological data, are a powerful tool for exploring viral dynamics as they provide a framework to quantify key characteristics of different variants and build an understanding of the drivers of inter-individual variation in response to infection. For example, previous within-host modelling studies of SARS-CoV-2 have enabled an understanding of the effect of covariates such as age, sex, and disease severity on viral load[24], the degree of heterogeneity between individuals[25], and the potential effect of antivirals and masking on viral load[26–30]. Models fitted to data from vaccine trials have suggested correlates of protection[31], while more theoretical immunological models have also been developed with the ultimate aim of understanding the interplay between the immune response and disease severity[32–34]. Studies linking the within- and between-host scales have improved the understanding of the relationship between Ct values and infectiousness[25,35], suggested characteristics of optimal testing regimes[36] and provided explanations for population-level epidemiological observations, e.g. the apparent reduction in viral load observed during the declining phase of an epidemic[37].

The studies mentioned above have all fitted their models to data from *in vivo* studies. While dynamics in humans are of ultimate interest, modelling viral kinetics and the immune response *in vivo* is

88 extremely complex. Moreover, studies in humans are often limited, with little or no information on

89 the timing and amount of the viral inoculum, sparse longitudinal observations, and often no available

90 measurements before the start of symptom onset[25,35]. *In vitro* studies offer a simplification of *in vivo*

91 dynamics, where both the inoculum and method of inoculation is controlled, and where some

92 components of the immune response – such as the adaptive immune response – are eliminated. Viral

93 load can be measured from the start of infection, which is important for estimating the growth rate

94 and basic reproduction number of the virus, which in turn can be used to assess the potential for load

95 variants to outcompete existing variants.

96 Here, using viral kinetics models calibrated against viral replication data generated through

97 experimental infection studies in primary human nasal epithelial cells (hNECs) and immortalised Calu-

98 3 lung cells, we characterise and compare the dynamics of Omicron and Delta viruses in each cell type

99 by quantifying key properties such as the basic reproduction number and growth rate, and by

100 exploring how these properties vary for different entry pathways, and in the presence and absence of

101 functional endosomal restriction factors.

102

Methods

Experimental Design/Data

105 Full details of the viral kinetics experiments conducted are provided in Peacock et al.[20] . In brief, Calu-

106 3 and primary human nasal epithelial cells (hNECs) were inoculated with Omicron BA.1 and

107 Delta/B.1.617.2 isolates at an MOI of 0.001 (Calu-3) or 0.05 (hNECs), and incubated for 1 hr at 37°C.

108 The inoculum was then removed and, in the case of Calu-3 cells, replaced with 1 mL serum-free

109 DMEM. For Calu-3 cells, 100 μL of supernatant was collected for titration at 18, 24, 48 and 72 hours

110 post-infection. For hNECs, at the same timepoints post-infection, the supernatant was collected by

111 adding 200 μL of serum-free DMEM to the apical surface, incubating for 10 minutes, and removing for

112 collection.

113 Additional experiments were performed to investigate the effect of Camostat mesylate (henceforth

114 referred to as Camostat) and Amphotericin B on viral kinetics. Camostat is a serine protease inhibitor

115 and thus inhibits TMPRSS2, while Amphotericin B inhibits the restriction of viral endosomal entry by

116 endosomal restriction factors such as IFITM proteins[38–40]. Cells were pre-treated both basolaterally

117 and apically with either 50 μM of Camostat, 1μM of Amphotericin B or no drug for 2 hours prior to

118 infection, and this concentration of drug was maintained in the basolateral media throughout the

119 experiment. Infections and collection of timepoints were performed as above.

120   All experiments were performed in triplicate. Infectious viral titres were quantified by plaque assay

121   and viral genome numbers were quantified by E gene RT-qPCR.

122   **Mathematical Models**

123   *Model 1*

124   To gain an initial understanding of the differences between the observed infection dynamics of the

125   Omicron and Delta variants across each cell type, we first developed a simple model of the viral

126   dynamics which assumed a single virus entry pathway for both variants. A simple schematic of the

127   model is provided in Figure 2. Model equations are in the Supplementary Methods.

128   Target cells T become infected at a rate β (target cell infection rate) per infectious virion (V_{Inf}). The

129   target cell infection rate is defined as the proportion of cells infected per day, per unit inoculum of 1

130   pfu/mL. Following an eclipse phase of mean duration of $1/\tau$ days, infectious cells (I) produce infectious

131   and non-infectious virus. Infectious virus (V_{Inf}), as measured by plaque-assay, and total (infectious and

132   non-infectious) virus (V_{RNA}), as measured by RT-qPCR, are produced at rates ω_{Inf} and ω_{RNA}

133   respectively. (While the RT-qPCR assay could detect viral RNA released from lysed cells as well as from

134   extracellular viral particles, the model assumes that all detected viral RNA originates from viral

135   particles.) The duration of the eclipse phase $1/\tau$ reflects the speed of a single viral replication cycle,

136   whereas the rate of viral production ω_{Inf} also reflects replication capacity. Infectious cells have a

137   mean lifespan of $1/\delta$ days, and infectious and non-infectious virus is assumed to decay at rates κ_{Inf}

138   and κ_{RNA} respectively, with additional loss due to entry into cells. Cells which express the ACE2

139   receptor, which is required for SARS-CoV-2 virus entry, are considered target cells.

140
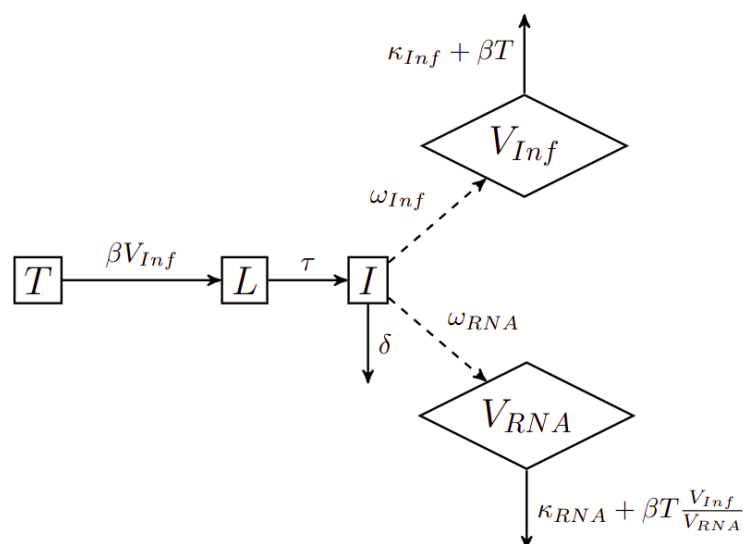
Figure 2: Compartmental diagram of model 1. Target cells T become infected at a rate β per infectious virion (V_{Inf}). Following an eclipse phase of mean duration of $1/\tau$ days, infectious cells (I) produce infectious virus as measured by plaque-assay (V_{Inf}) and total virus as measured by qPCR (V_{RNA}) at rates ω_{Inf} and ω_{RNA} respectively. Infected cells have a mean lifespan of $1/\delta$ days, and infectious and total virus are assumed to decay at rates κ_{Inf} and κ_{RNA} respectively.
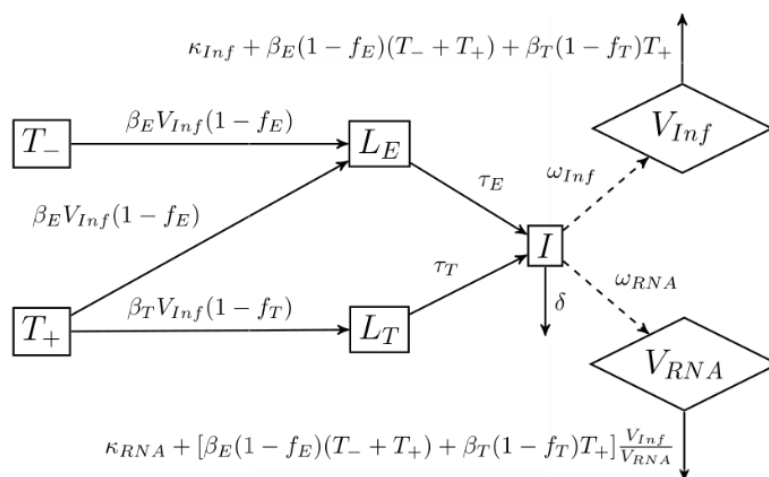
Model 2

The experimental data showed that while Delta can only enter ACE2$^+$ cells by utilizing the TMPRSS2 protein, Omicron can enter these cells both through TMPRSS2- dependent and TMPRSS2-independent pathways. Thus, in Model 2 we modify Model 1 to account for the two possible cell entry pathways, where TMPRSS2-independent pathways can be used to infect all ACE2$^+$ cells, and TMPRSS2-dependent pathways can only infect ACE2$^+$ TMPRSS2$^+$ cells. We assume that all ACE2$^+$ cells become infected through TMPRSS2-independent pathways at a rate β_E per infectious virion (V_{Inf}) and that ACE2$^+$ TMPRSS2$^+$ target cells (T_+) also become infected through TMPRSS2-dependent pathways at a rate β_T per infectious virion. We assume that endosomal restriction factors decrease the infectivity through the TMPRSS2-independent pathways by a factor f_E, and through TMPRSS2-dependent pathways by a factor f_T. Cells infected through TMPRSS2-independent and TMPRSS2-dependent pathways (L_E and L_T respectively) undergo eclipse phases of mean duration $1/\tau_E$ and $1/\tau_T$ days respectively. Following the eclipse phase, infectious cells (I) behave as per Model 1. The flow diagram of Model 2 is described in Figure 3.

163

Figure 3: Compartmental diagram for Model 2. ACE2⁺ TMPRSS2⁻ target cells (T₋) become infected through TMPRSS2-independent pathways at a rate β_E per infectious virion (V_{Inf}). ACE2⁺ TMPRSS2⁺ target cells (T₊) become infected through TMPRSS2-independent pathways at a rate β_E per infectious virion, and through TMPRSS2 -dependent pathways at a rate β_T per infectious virion. Endosomal restriction factors decrease the infectivity through TMPRSS2-independent pathways by a factor f_E, and through TMPRSS2-dependent pathways by a factor f_T. Cells infected through TMPRSS2-independent and TMPRSS2-dependent pathways (L_E and L_T respectively) undergo eclipse phases of mean duration $1/\tau_E$ and $1/\tau_T$ days respectively. Following the eclipse phase, infectious cells (I) behave as per Model 1.

Model 2 is fitted to hNEC and Calu-3 data without drug, in the presence of Camostat, in the presence of Amphotericin B, and in the presence of both drugs. For each virus strain/cell type combination, all data (with and without drugs) is fitted simultaneously. Camostat is assumed to completely inhibit TMPRSS2-dependent pathways (we set $\beta_T = 0$); although Camostat also inhibits other serine proteases, but as TMPRSS2 is the main serine protease involved in SARS-CoV-2 virus entry, and because the activation of S2' in TMPRSS2-independent pathways likely occurs by cathepsin proteases rather than serine proteases, for simplicity we assume that Camostat does not affect TMPRSS2-independent pathways. Amphotericin B is assumed to completely remove endosomal restriction (we set $f_E = f_T = 0$).

Inferential framework

We calibrated the models to the observed data in a Bayesian inferential framework using Markov Chain Monte Carlo (MCMC) methods. In the results, we reported the median and 95% credible interval (CrI) of the parameter estimates. Full details of the model fitting algorithms are provided in the Supplementary Methods.
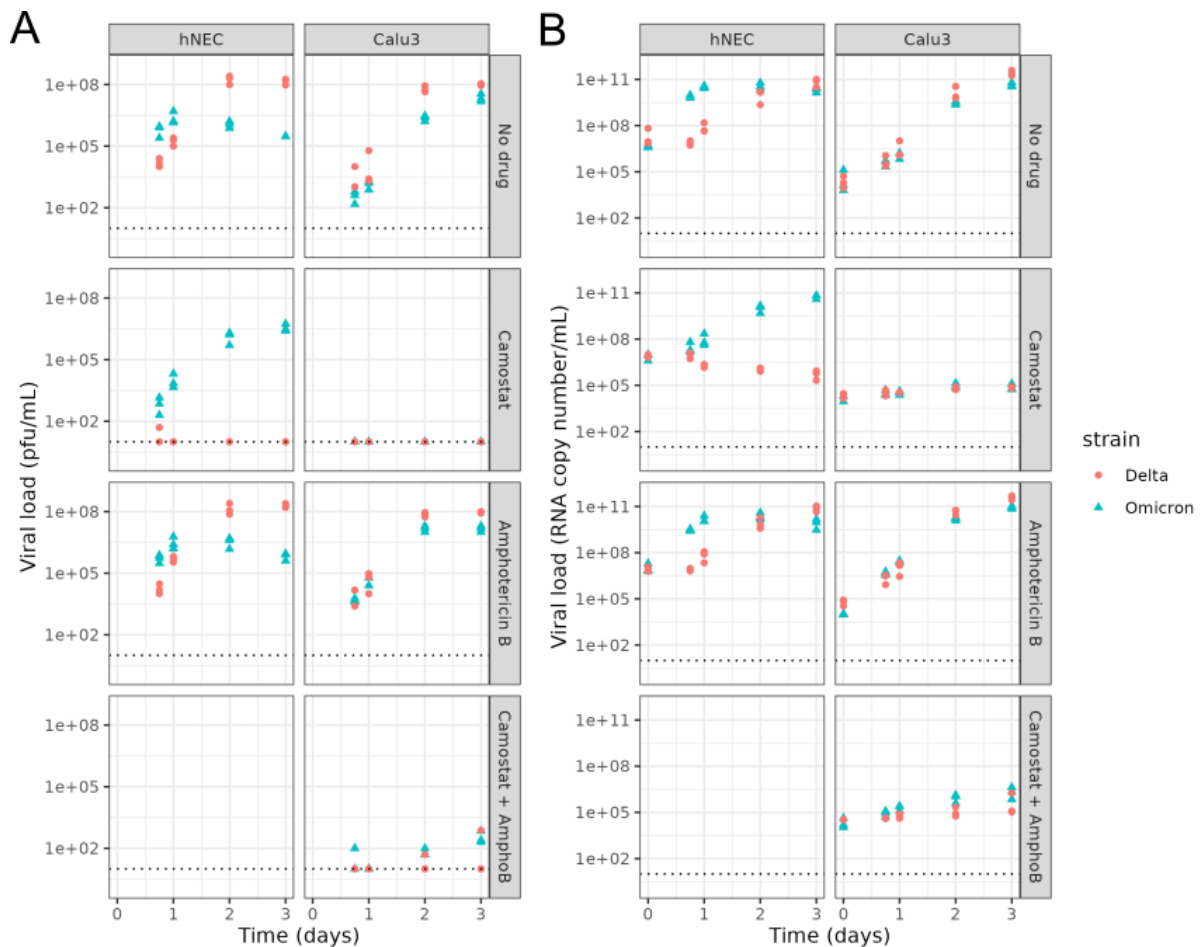
Results

Data Description

Figure 4: Summary of Data. (A) Infectious viral load (pfu/mL) quantified by plaque assay and (B) RNA copy number/mL quantified by RT-qPCR for Omicron (blue triangles) and Delta (red dots) for different cell types (columns) and drug treatments (rows). The dotted line shows the limit of detection; markers on the lines represent measurements below the limit of detection. Cells were infected on day 0.

Figure 4 summarises the study data. In control wells with no drug, temporal trends in viral growth varied both between strains and cell type. In hNECs, Omicron grew more rapidly than Delta, with viral load peaking by 1 day post infection (p.i.) for Omicron, compared with 2 days p.i. for Delta. However, despite this initial growth advantage, viral load was higher for Delta compared to Omicron at 3 days p.i.. In Calu-3 cells, the peak in viral load was observed 2-3 days p.i. for both Omicron and Delta. In contrast with hNECs where the strain corresponding to the highest viral load was dependent on measurement time, infectious and non-infectious viral load was higher for Delta than Omicron across all time points for Calu-3 cells.

In the presence of the drug Camostat which inhibits serine proteases, and thus TMPRSS2-dependent pathways, replication of Delta was severely inhibited in hNECs with no detectable increase in virus throughout the course of the experiment. In contrast, Omicron successfully replicated in hNECs in the presence of Camostat, albeit at a slower rate than in untreated wells. However, similar levels of viral

209   load were obtained by 2-3 days p.i. in both the presence and absence of Camostat. For both strains,

210   the presence of Amphotericin B had little impact on viral load dynamics in hNECs. In Calu-3 cells,

211   infectious virus was not detected at any point for either Omicron or Delta in the presence of Camostat.

212   In the presence of the drug Amphotericin B which is described as specifically inhibiting endosomal

213   restriction[22,39], Omicron infectious viral titres were consistently higher than in control wells, until 3

214   days p.i. when titres became similar. Delta geometric mean infectious viral titres were similar with

215   and without Amphotericin B.

216

217   Experiments with both drugs combined were only performed for Calu-3 cells. For both virus strains,

218   the infectious viral load was below the limit of detection in the presence of Camostat only. Adding

219   Amphotericin B raised the infectious viral load to above the limit of detection for all replicates for

220   Omicron, but only for some replicates for Delta (Figure 4).
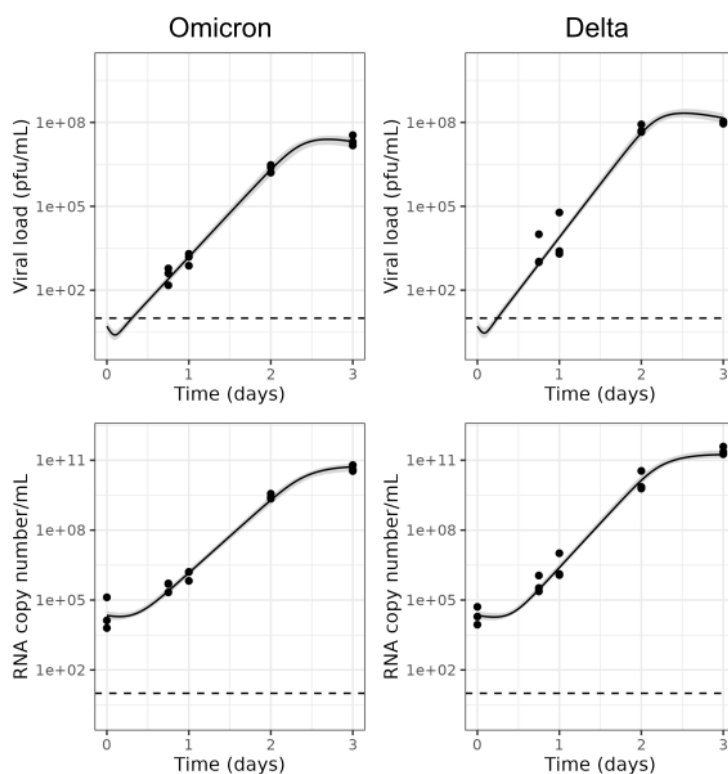
221

222   **Viral Fitness**

223

224   **Model 1**
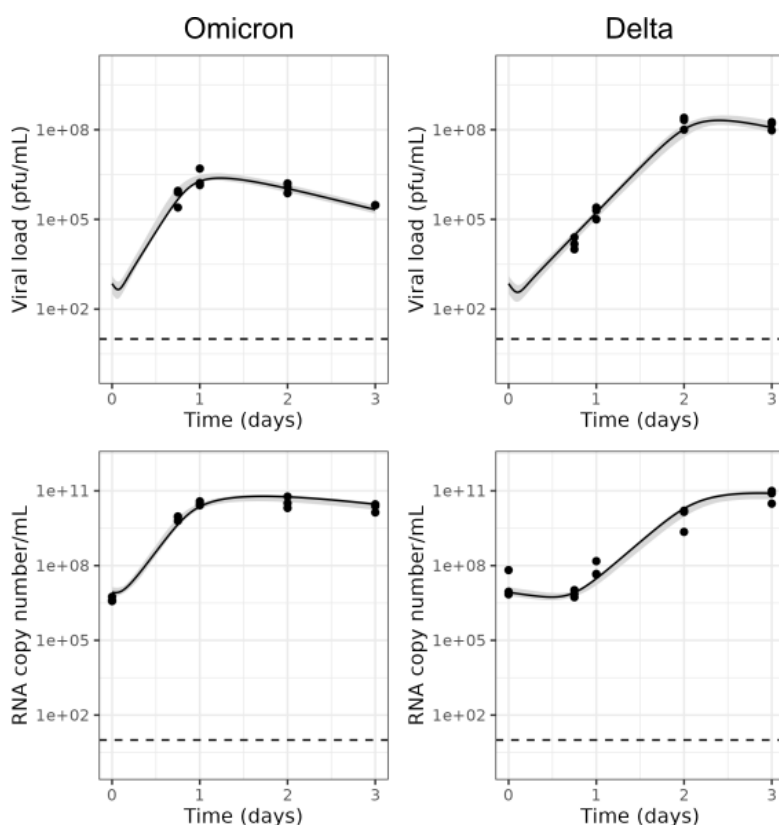
225

226   **Figure 5: Model 1 fits to data from hNECs without drugs.** Dots show the data, black lines show the maximum likelihood
227   fit, shaded areas show the 95% credible interval (CrI) and dotted lines show the limit of detection.

Figure 6: Model 1 fits to data from Calu-3 cells without drugs. Dots show the data, black lines show the maximum
likelihood fit, shaded areas show the 95% credible interval (CrI) and dotted lines show the limit of detection.

For both Omicron and Delta, the simple model (Model 1) captured the viral dynamics observed in
control wells of hNECs and Calu-3 cells (Figures 5, 6). For hNECs, we estimated a higher target cell
infection rate β for Omicron relative to Delta (2.13e-05 (95% CrI: 1.54e-05, 3.07e-05) cell (pfu/mL)$^{-1}$
day^{-1} for Omicron, 8.89e-08 (95% CrI: 5.91e-08, 1.28e-07) cell (pfu/mL)$^{-1}$ day^{-1} for Delta), but a lower
infectious virus production rate ω_{Inf} for Omicron relative to Delta (4.07e+03 (95% CrI: 3.13e+03,
5.50e+03) pfu/mL cell^{-1} day^{-1} for Omicron, 3.42e+05 (95% CrI: 2.41e+05, 5.04e+04) pfu/mL cell^{-1} day^{-1}
for Delta). All estimated parameters are presented in Supplementary Table 2. These results suggest
an approximately 1.5-fold difference in the growth rate between these strains in hNECs, with a growth
rate of 11.61 day^{-1} (95% CrI: 10.43,12.99) for Omicron and 6.87 day^{-1} (95% CrI: 6.33,7.50) for Delta.
Furthermore, we estimated a higher basic reproduction number (R_0) for Omicron (65.04 (95% CrI:
51.94, 82.71)) compared with Delta (23.13 (95% CrI: 19.91, 27.23)), thereby suggesting an overall
increase in viral fitness of Omicron relative to Delta in hNECs.

For Calu-3 cells, we estimated a higher target cell infection rate for Omicron than Delta (9.23e-07 (95%
CrI: 6.17e-07, 1.36e-06) cell (pfu/mL)$^{-1}$ day^{-1} for Omicron, 1.42e-07 (95% CrI: 9.80e-08, 2.05e-07) cell

247 (pfu/mL)$^{-1}$ day^{-1} for Delta) and lower infectious virus production rate for Omicron than Delta (4.13e+02

248 (95% CrI: 2.85e+02,6.07e+02) cell (pfu/mL)$^{-1}$ day^{-1} for Omicron, 3.73e+03 (95% CrI:

249 2.67e+03,5.32e+03) cell (pfu/mL)$^{-1}$ day^{-1} for Delta). In contrast with hNECs, our results indicate an

250 overall increase in viral fitness of Delta relative to Omicron in Calu-3 cells as we estimated a higher

251 basic reproduction number of Delta (36.67 (95% CrI: 33.69, 39.81)) compared to Omicron (24.23 (95%

252 CrI: 22.14, 26.70)) in this cell type. In addition, we estimated a larger growth rate of Delta relative to

253 Omicron in Calu-3 cells, with a growth rate of 8.78 day^{-1} (95% CrI: 8.40, 9.15) for Delta compared with

254 7.25 day^{-1} (95% CrI: 6.86, 7.60) for Omicron (for details see Supplementary Table 2).

255

256 For both cell types, the target cell infection rate (β), which is positively correlated with the probability

257 of a virion successfully infecting a cell, was higher for Omicron than Delta. The infectious virus

258 production rate (ω_{Inf}), which is directly proportional to the burst size (the total number of infectious

259 virions produced by one infected cell), was higher for Delta than Omicron. However, the magnitude

260 of each of these differences meant that the basic reproduction number and growth rate, which are

261 both functions of the target cell infection rate and the infectious virus production rate (see

262 Supplementary Methods), were higher for Omicron in hNECs, but higher for Delta in Calu-3 cells
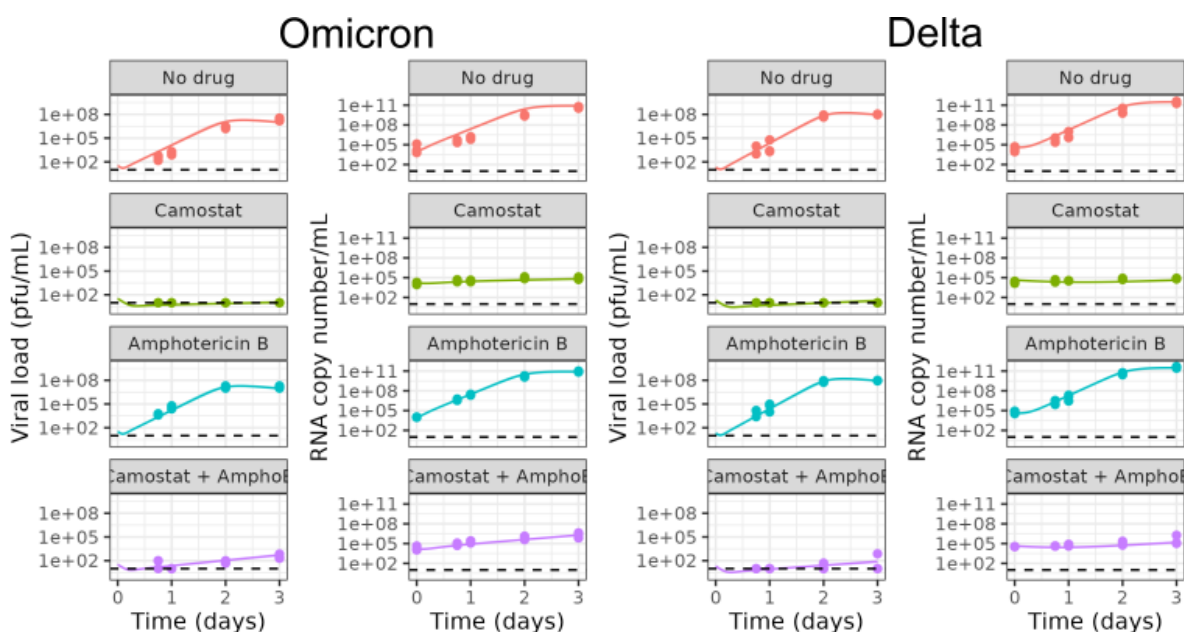
263 (Supplementary Table 2).

264

265 **Model 2**
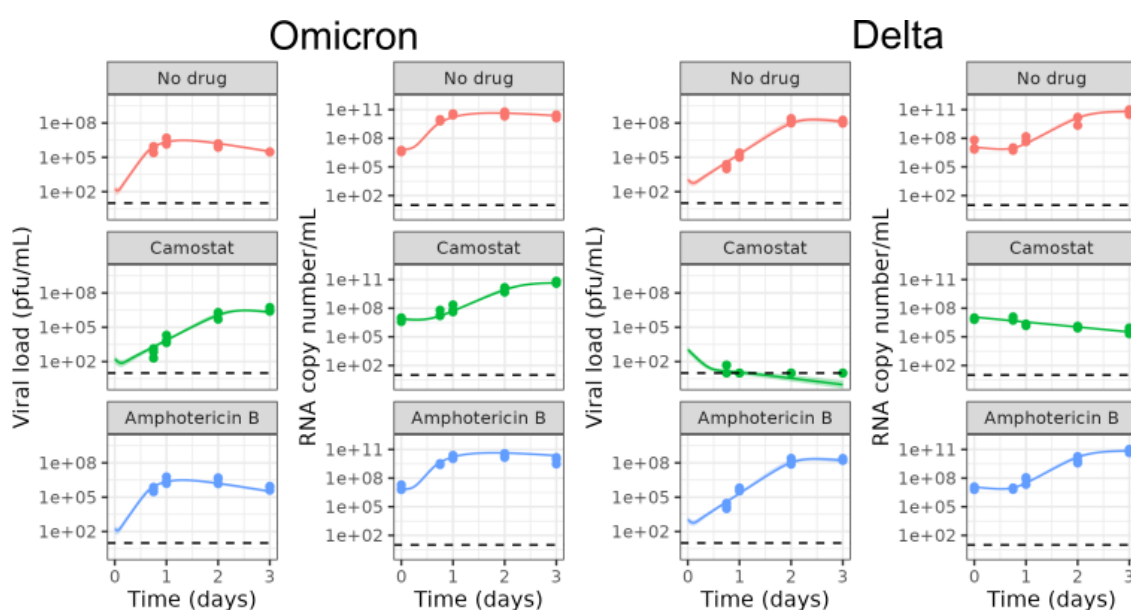
266

267 **Figure 7. Model 2 fits to data from hNECs with and without drugs.** Dots show the data, black lines show the maximum
268 likelihood fit, shaded areas show the 95% credible interval (CrI) and dotted lines show the limit of detection. Markers on
269 the lines represent measurements below the limit of detection.

270

271

272 **Figure 8. Model 2 fits to data from Calu-3 cells with and without drugs**. Dots show the data, black lines show the
273 maximum likelihood fit, shaded areas show the 95% credible interval (CrI) and dotted lines show the limit of detection.
274 Markers on the lines represent measurements below the limit of detection.

275

276 When fitting Model 2 to the data, we found the same qualitative result that Omicron's R_0 is higher

277 than Delta's in hNECs, but lower in Calu-3 cells (Figures 7 and 8). In hNECs, R_0 for Omicron was

278 estimated to be 106.59 (95% CrI: 85.92, 134.72), while for Delta it was estimated to be 21.61 (95% CrI:

279 18.97, 25.30). In Calu-3 cells, R_0 for Omicron was estimated to be 16.53 (95% CrI: 15.15, 17.99), and

280 for Delta was estimated to be 27.87 (95% CrI: 25.60, 30.34). R_0 estimates were comparable between

281 Models 1 and 2, except for Omicron in hNECs, where the R_0 estimates obtained with Model 2 were

282 higher. This discrepancy occurred because Model 2 predicts that Omicron can use both TMPRSS2-

283 dependent and TMPRSS2-independent pathways in hNECs (see next section), whereas for all other

284 strain and cell combinations only TMPRSS2-dependent pathways are active. When only TMPRSS2-

285 dependent pathways are active, then in the absence of drug, Models 1 and Model 2 are the same. All

286 parameter estimates are presented in Supplementary Table 1.

287

288 **Role of Cell Entry Pathways**

289

290 As Camostat inhibits serine proteases including TMPRSS2, Camostat-sensitive viruses must be able to

291 use TMPRSS2-independent pathways for cell entry; thus, the fit of Model 2 to the data in the presence

292 of Camostat provides information on the role of cell entry pathways. We found that in hNECs, Omicron

293 was able to utilise both TMPRSS2-dependent and TMPRSS2-independent pathways. The median

294   estimates of R_{0T} and R_{0E} were 92.13 (95% CrI: 72.95, 118.27) and 15.44 (95% CrI 12.86, 18.52)

295   respectively (Supplementary Table 3). On the other hand, in hNECs, Delta was unable to effectively

296   use TMPRSS2-independent pathways, as $R_{0E} < 1$ (median 0.15, 95% CrI: (0.07, 0.30)). In Calu-3s,

297   neither virus was able to use TMPRRS2-independent pathways effectively. R_{0E} was estimated to be

298   slightly greater than 1 for both Omicron (median 1.34 (95% CrI: 1.14, 1.55)) and Delta (median 1.71

299   (95% CrI: 1.47, 1.98)) but these small values of R_0 are insufficient for the viral load to exceed the limit

300   of detection during the time course of the experiment (Figure 8 Camostat panels). Note that for

301   Omicron in hNECs, the estimate for R_{0T} is comparable to the overall R_0 for Model 1. This is because

302   the increase in viral load due to TMPRSS2-dependent pathways is much faster than through TMPRSS2-

303   independent pathway, so the TMPRSS2-dependent pathway is the main contributor to the initial

304   exponential increase, from which Model 1 estimates R_0.

305

306   It has been suggested that Omicron's use of TMPRRS2-independent pathways explains its fitness

307   advantage over Delta[12,16,17]. However, even the TMPRSS2-specific basic reproduction number is higher

308   for Omicron than Delta in hNECs, with a median R_{0T} equal to 92.13 (95% CrI: 72.95, 118.27) for

309   Omicron compared to 21.46 (95% CrI:18.89, 25.05) for Delta. In fact, R_{0T} alone for Omicron is greater

310   than the overall R_0 for Delta. Therefore, it is primarily Omicron's more efficient use of TMPRSS2-

311   dependent pathways, rather than its utilisation of TMPRSS2-independent pathways, which gives it a

312   fitness advantage over Delta in hNECs.

313

314   **Role of endosomal restriction**

315

316   As Amphotericin B inhibits restrictions to virus entry imposed by endosomal restriction factors, the fit

317   of Model 2 to the Amphotericin B data provides information on the role of endosomal restriction

318   factors in shaping the viral dynamics observed. The parameters f_E and f_T capture the degree of

319   inhibition of TMPRSS2-independent and TMPRSS2-dependent pathways by endosomal restriction

320   factors respectively, and Amphotericin B is assumed to set these parameters to 0. Comparing across

321   cell types, inhibition by endosomal restriction factors was higher in Calu-3 cells than hNECs across all

322   strains and pathways (higher values of f_E and f_T for Calu-3 cells compared to hNEC cells in

323   Supplementary Table 4), with the exception of TMPRSS2-independent pathways for Delta, where f_E

324   could not be estimated precisely. Inhibition was similar for both Omicron and Delta in hNECs, but

325   Omicron was more inhibited by endosomal restriction factors than Delta in Calu-3 cells for both

326   pathways (higher values of f_E and f_T for Omicron than Delta in Calu-3 cells in Supplementary Table

327   4). Comparing across pathways, f_E and f_T were similar for each virus strain in hNECs, but in Calu-3

328   cells, f_E was higher than f_T for both virus strains, suggesting more inhibition of TMPRSS2-independent

329   pathways than of TMPRSS2-dependent pathways.

330

331   Given that TMPRSS2-independent pathways are susceptible to inhibition by endosomal restriction

332   factors, and that previous variants were not able to use endosomal restriction pathways, one may

333   hypothesise that Omicron has overcome endosomal restriction in hNECs, and that TMPRSS2-

334   independent pathways would also be accessible by other virus-cell combinations if endosomal

335   restriction were lifted. However, we predict that even if endosomal restriction is lifted for the three

336   other virus-cell combinations (as per the Amphotericin B experiments) R_{0EX} remains low.   This

337   suggests that other factors contribute to Omicron's increased use of TMPRSS2-independent pathways

338   in hNECs. We predict that in the absence of endosomal restriction factors, Omicron would still have a

339   higher overall basic reproduction number and growth rate than Delta in hNECs, but these quantities

340   would be similar between variants in Calu-3 cells (R_{0X} in Supplementary Table 3 and r_X in

341   Supplementary Table 6).

342

343   **Changing the assumed eclipse phase duration**

344

345   A caveat of the above results is that we have fixed the length of the eclipse phase. The eclipse phase

346   in this model reflects the speed of viral replication with the cell. To date, studies which have measured

347   the duration of the eclipse phase in the SARS-CoV-2 viral life cycle have used viruses which enter target

348   cells through TMPRSS2-dependent pathways only[41,42]. Thus, the duration of the eclipse phase for

349   TMPRSS2-independent pathways is unclear and our knowledge of this component of the viral life cycle

350   is limited. To address this, we conducted a sensitivity analysis around the duration of the eclipse phase.

351   In Model 1, τ was set to 6, 4, or 2 day^{-1}. In Model 2, τ_T was set to 6, 4 or 2 day^{-1}, and τ_E was set to 4,

352   2 or 1 day^{-1}. We found that for Model 1, regardless of the duration of the eclipse phase assumed – as

353   long as it was the same between strains – Omicron had a higher R_0 than Delta in hNECs, and Delta

354   had a higher R_0 than Omicron in Calu-3 cells (Supplementary Table 4). Also, all estimated R_0 values

355   decreased as the duration of the eclipse phase decreased, as expected theoretically. This is because

356   if, at the start of infection, cells start producing virus sooner due to a short eclipse phase, then each

357   individual infected cell needs to lead to fewer secondary infections to reproduce the dynamics

358   observed. Similarly, for Model 2, we found that regardless of the values of τ_E and τ_T, as long as these

359   were assumed to be the same between strains, Omicron had a higher R_0 than Delta in hNECs, and

360   Delta had a higher R_0 than Omicron in Calu-3 cells; only Omicron in hNECs used TMPRSS2-independent

361   pathways efficiently; and endosomal restriction only had a significant effect in Calu-3 cells

362   (Supplementary Table 5). However, allowing the duration of the eclipse phase to be different between

363   strains, no longer allows us to draw conclusions about whether R_0 is greater for Omicron or Delta

364   (Supplementary Tables 3 and 5). On the other hand, estimates of the growth rate r only varied slightly

365   with the assumed duration of the eclipse phase for both models (Supplementary Tables 4 and 6).

366

367

Discussion

By fitting a simple within-host model to viral kinetics data for Omicron and Delta in hNECs and Calu-3 cells we found that Omicron has a fitness advantage over Delta in hNECs, but Delta has a fitness advantage over Omicron in Calu-3 cells, as measured by both the growth rate and basic reproduction number of the virus. These findings are consistent with previously published studies showing faster replication of Omicron compared with Delta in human nasal epithelial cells[14,16], and faster replication of Delta compared with Omicron in the ex vivo explant cultures of human lungs[12] and Calu-3 cells[43].

We estimated that Omicron had a higher rate of infection β in both cell types, which could be linked to increased ACE2 binding affinity, likely due to mutations in the spike protein. Evidence is mixed as to whether Omicron has a higher ACE2 binding affinity than Delta. Cameroni et al.[44] found that Omicron has a higher human ACE2 binding affinity than Delta, but Mannar et al.[45] found that ACE2 binding affinity is similar for Omicron and Delta, though higher than the ancestral strain. On the other hand, Zhang et al.[46] found that the Omicron spike protein required a higher level of ACE2 than Delta for efficient membrane fusion. We also estimated that Omicron had a lower rate of infectious virus production ω_{Inf} than Delta for both cell types. Changes to the rate of viral production could be due to mutations in either spike or non-spike proteins. The basic reproduction number is positively correlated with both the rate of infection β and the rate of infectious virus production ω_{Inf} in our models. In hNECs, the increase in the rate of infection β for Omicron was greater than the decrease in infectious virus production ω_{Inf}, resulting in a larger basic reproduction number and growth rate for Omicron compared to Delta; the converse was true in Calu-3 cells.

Previous studies have proposed that TMPRSS2-independent pathways which are only available to Omicron are responsible for its faster growth in hNECs. Our study found that Omicron can use TMPRSS2-independent pathways in hNECs, consistent with the previous studies. However, the growth rate and basic reproduction number for TMPRSS2-independent pathways was low and insufficient to explain the overall fitness advantage for Omicron over Delta in hNECs. On the other hand, the growth rate and basic reproduction number for TMPRSS2-dependent pathways was also higher for Omicron than Delta in hNECs and was sufficient to explain the overall fitness advantage. Evidence for the continued importance of TMPRSS2-dependent pathways for Omicron was provided by a study by Metzdorf et al.[47] which found that the growth of Omicron in the nose and lung was attenuated in TMPRSS2 knockout mice. In Calu-3 cells, neither Omicron nor Delta can use TMPRSS2-independent pathways, thereby providing further insight into how these viruses use different pathways to enter target cells.

400   We estimated the degree of inhibition in viral growth imposed by endosomal restriction factors by

401   fitting our model to data where the cells were treated with Amphotericin B, as Amphotericin B inhibits

402   the action of endosomal restriction factors. The main hypotheses tested were i) whether Omicron

403   was able to evade endosomal restriction in hNECs; ii) whether this evasion enabled Omicron to use

404   TMPRSS2-independent pathways; and iii) whether this was responsible for Omicron's growth

405   advantage. We found that the fitness of Delta in hNECs without endosomal restriction, as measured

406   by the basic reproduction number R_{0X} and the growth rate r_X, was still lower than that of Omicron in

407   hNECs with endosomal restriction. Hence, reduced endosomal restriction alone do not explain

408   Omicron's fitness advantage in hNECs. Although we were able to quantify the degree of inhibition by

409   endosomal restriction factors for both pathways for Omicron in hNECs, we were unable to do so for

410   Delta, as doing so requires either the infectious viral load to be above the limit of detection in the

411   presence of Camostat (as was the case for Omicron in hNECs), or requires data on viral growth in the

412   presence of both drugs (as was the case in Calu-3 cells). Hence, we were unable to make a direct

413   comparison at a pathway-specific level between Omicron and Delta in hNECs. In Calu-3 cells, we found

414   that Omicron was more inhibited by endosomal restriction factors than Delta, for either TMPRSS2-

415   dependent or TMPRSS2-independent pathways.

416   The model has several limitations. First, we fixed the infected cell death rate, the rate at which viruses

417   lose infectivity, the RNA degradation rate and the duration of eclipse phases, according to values from

418   the literature. It is currently unclear whether the duration of the eclipse phase differs between

419   variants. To test this, we conducted a sensitivity analysis where the model was fitted assuming

420   different lengths of the eclipse phase. This sensitivity analysis showed that if eclipse phase lengths

421   were assumed to be the same between Omicron and Delta, while the estimated values of R_0 changed

422   with the assumed length of the eclipse phase, the trends and relationships in R_0 and the growth rate

423   estimates r between Omicron and Delta (for example, that Omicron has a higher R_0 and growth rate

424   estimate r than Delta in hNECs) remained unchanged. Allowing the eclipse phase to be different

425   between strains, no longer allows us to draw conclusions about whether R_0 is greater for Omicron or

426   Delta (Supplementary Tables 3 and 5), but the differences in r are robust. This result reflects the

427   finding that if the eclipse phase is allowed to vary, the growth rate r is identifiable but R_0 is not. Future

428   studies could measure the duration of the eclipse phase for each cell type and virus strain using single-

429   cycle growth kinetics experiments.

430   We also did not test the effect of changing the assumed values of the infected cell or virus decay rates.

431   Studies have shown that Omicron survives for longer on surfaces than the ancestral strain[48] and

432   Delta[49], so it is plausible that extracellular virus may also differ in stability in our experiments.

433   Moreover, fixing the parameters using values from previous studies may underestimate the

434   uncertainty in R_0 and r.

435   Another limitation of the model is that it assumes 100% effectiveness for both drugs. Assuming 100%

436   effectiveness of Camostat means interpreting all remaining viral growth as due to TMPRSS2-

437   independent pathways, so if the drug is less than 100% effective, the contribution of TMPRSS2-

438   independent pathways will be overestimated. Assuming 100% effectiveness of Amphotericin B means

439   interpreting viral growth in the presence of Amphotericin B as the viral growth in the complete

440   absence of endosomal restriction. If the drug were less than 100% effective, the viral load in the

441   complete absence of endosomal restriction could be higher than that suggested by the data, so the

442   effect of endosomal restriction would be underestimated.

443   Last, the structure of the model is such that the initial growth rate is independent of the inoculum

444   size. It is plausible that differences in growth rate between hNECs and Calu-3 cells observed in the

445   experiments were partly due to the differing inoculum sizes used, as a higher inoculum could, for

446   example, trigger endosomal restriction factors more quickly – an effect which was not modelled. A

447   higher multiplicity of infection (MOI) was used for hNECs as a lower MOI did not always successfully

448   infect these primary cells; repeating the Calu-3 experiments at the same higher MOI would strengthen

449   confidence in our comparison between cell types.

450   The models developed in this study can inform future studies using more complex models. Models

451   capturing more immune components and how the virus spreads within the host are useful for

452   understanding contributors to disease severity and the effects of antivirals[32–34], but because they have

453   many parameters, it is often difficult to determine their values by fitting them to data. This study can

454   help parameterize these models.

455   The models developed in this study can be applied to different SARS-CoV-2 virus strains to help

456   enhance our understanding of transmission potential of new strains as the virus continues to evolve.

457   While between-strain differences in the speed of viral replication is typically assessed by comparing

458   viral titre measurements at individual timepoints, adopting a mathematical modelling approach using

459   longitudinal timepoints enables us to estimate key characteristics of different strains such as the

460   growth rate and viral fitness, thus providing a deeper insight into the factors shaping observed

461   differences in viral dynamics at the individual and population level.

462

References

1. WHO. Classification of Omicron (B.1.1.529): SARS-CoV-2 Variant of Concern. *Who* 1 https://www.who.int/news/item/26-11-2021-classification-of-omicron-(b.1.1.529)-sars-cov-2-variant-of-concern (2021).

2. GISAID. GISAID - hCov19 Variants. *Gisaid* https://gisaid.org/hcov19-variants/ (2022).

3. WHO. Tracking SARS-CoV-2 variants. *Who* https://www.who.int/en/activities/tracking-SARS-Co Preprint at (2021).

4. Viana, R. *et al.* Rapid epidemic expansion of the SARS-CoV-2 Omicron variant in southern Africa. *Nature* **603**, 679–686 (2022).

5. Cele, S. *et al.* Omicron extensively but incompletely escapes Pfizer BNT162b2 neutralization. *Nature* **602**, 654–656 (2022).

6. Planas, D. *et al.* Considerable escape of SARS-CoV-2 Omicron to antibody neutralization. *Nature* **602**, 671–675 (2022).

7. Cao, Y. *et al.* Omicron escapes the majority of existing SARS-CoV-2 neutralizing antibodies. *Nature* **602**, 657–663 (2022).

8. Dejnirattisai, W. *et al.* SARS-CoV-2 Omicron-B.1.1.529 leads to widespread escape from neutralizing antibody responses. *Cell* **185**, 467-484.e15 (2022).

9. Andrews, N. *et al.* Covid-19 Vaccine Effectiveness against the Omicron (B.1.1.529) Variant. *New England Journal of Medicine* **386**, 1532–1546 (2022).

10. Nyberg, T. *et al.* Comparative analysis of the risks of hospitalisation and death associated with SARS-CoV-2 omicron (B.1.1.529) and delta (B.1.617.2) variants in England: a cohort study. *The Lancet* **399**, 1303–1312 (2022).

11. Wolter, N. *et al.* Early assessment of the clinical severity of the SARS-CoV-2 omicron variant in South Africa: a data linkage study. *The Lancet* **399**, 437–446 (2022).

12. Hui, K. P. Y. Y. *et al.* SARS-CoV-2 Omicron variant replication in human bronchus and lung ex vivo. **603**, (2022).

13. Willett, B. J. *et al.* SARS-CoV-2 Omicron is an immune escape variant with an altered cell entry pathway. *Nature Microbiology 2022 7:8* **7**, 1161–1179 (2022).

14. Barut, G. T. *et al.* The spike gene is a major determinant for the SARS-CoV-2 Omicron-BA.1 phenotype. *Nat Commun* **13**, 1–14 (2022).

15. Lyngse, F. P. *et al.* Household transmission of the SARS-CoV-2 Omicron variant in Denmark. *Nat Commun* **13**, 5573 (2022).

16. Willett, B. J. *et al.* SARS-CoV-2 Omicron is an immune escape variant with an altered cell entry pathway. *Nat Microbiol* (2022) doi:10.1038/s41564-022-01143-7.

17. Meng, B. *et al.* Altered TMPRSS2 usage by SARS-CoV-2 Omicron impacts infectivity and fusogenicity. *Nature 2022 603:7902* **603**, 706–714 (2022).

18. Suzuki, R. *et al.* Attenuated fusogenicity and pathogenicity of SARS-CoV-2 Omicron variant. *Nature* **603**, 700–705 (2022).

19. Hoffmann, M. *et al.* SARS-CoV-2 Cell Entry Depends on ACE2 and TMPRSS2 and Is Blocked by a Clinically Proven Protease Inhibitor. *Cell* **181**, 271-280.e8 (2020).

20. Peacock, T. P. *et al.* The altered entry pathway and antigenic distance of the SARS-CoV-2 Omicron variant map to separate domains of spike protein. *bioRxiv* 2021.12.31.474653 (2022) doi:10.1101/2021.12.31.474653.

21. Winstone, H. *et al.* The Polybasic Cleavage Site in SARS-CoV-2 Spike Modulates Viral Sensitivity to Type I Interferon and IFITM2. *J Virol* **95**, e02422-20 (2021).

22. Peacock, T. P. *et al.* The furin cleavage site in the SARS-CoV-2 spike protein is required for transmission in ferrets. *Nat Microbiol* **6**, 899–909 (2021).

23. Khan, H. *et al.* TMPRSS2 promotes SARS-CoV-2 evasion from NCOA7-mediated restriction. *PLoS Pathog* **17**, e1009820 (2021).

24. Challenger, J. D. *et al.* Modelling upper respiratory viral load dynamics of SARS-CoV-2. *BMC Med* **20**, 25 (2022).

25. Ke, R., Zitzmann, C., Ho, D. D., Ribeiro, R. M. & Perelson, A. S. In vivo kinetics of SARS-CoV-2 infection and its relationship with a person's infectiousness. *Proc Natl Acad Sci U S A* **118**, e2111477118 (2021).

26. Gonçalves, A. *et al.* Timing of Antiviral Treatment Initiation is Critical to Reduce SARS-CoV-2 Viral Load. *CPT Pharmacometrics Syst Pharmacol* **9**, 509–514 (2020).

27. Gonçalves, A. *et al.* SARS-CoV-2 viral dynamics in non-human primates. *PLoS Comput Biol* **17**, (2021).

28. Perelson, A. S. & Ke, R. Mechanistic Modeling of SARS-CoV-2 and Other Infectious Diseases and the Effects of Therapeutics. *Clin Pharmacol Ther* **109**, 829–840 (2021).

29. Koelle, K. *et al.* Masks Do No More Than Prevent Transmission: Theory and Data Undermine the Variolation Hypothesis. Preprint at https://doi.org/10.1101/2022.06.28.22277028 (2022).

30. Ito, K., Piantham, C. & Nishiura, H. Relative instantaneous reproduction number of Omicron SARS-CoV-2 variant with respect to the Delta variant in Denmark. *J Med Virol* **94**, 2265–2268 (2022).

31. Alexandre, M. *et al.* Modelling the response to vaccine in non-human primates to define SARS-CoV-2 mechanistic correlates of protection. *Elife* **11**, e75427 (2022).

32. Jenner, A. L. *et al.* COVID-19 virtual patient cohort suggests immune mechanisms driving disease outcomes. *PLoS Pathog* **17**, e1009753 (2021).

33. Rowlatt, C. F. *et al.* Modelling the within-host spread of SARS-CoV-2 infection, and the subsequent immune response, using a hybrid, multiscale, individual-based model. Part I: Macrophages. *bioRxiv* (2022) doi:10.1101/2022.05.06.490883.

34. Getz, M. *et al.* Iterative community-driven development of a SARS-CoV-2 tissue simulator. *bioRxiv* (2021) doi:10.1101/2020.04.02.019075.

35. Marc, A. *et al.* Quantifying the relationship between SARS-CoV-2 viral load and infectiousness. *Elife* **10**, e69302 (2021).

36. Larremore, D. B. *et al.* Test sensitivity is secondary to frequency and turnaround time for COVID-19 screening. *Sci Adv* **7**, eabd5393 (2021).

37. Hay, J. A. *et al.* Estimating epidemiologic dynamics from cross-sectional viral load distributions. *Science (1979)* **373**, eabh0635 (2021).

38. Brass, A. L. *et al.* The IFITM Proteins Mediate Cellular Resistance to Influenza A H1N1 Virus, West Nile Virus, and Dengue Virus. *Cell* **139**, 1243–1254 (2009).

39. Lin, T.-Y. *et al.* Amphotericin B Increases Influenza A Virus Infection by Preventing IFITM3-Mediated Restriction. *Cell Rep* **5**, 895–908 (2013).

40. Qian, J. *et al.* Primate lentiviruses are differentially inhibited by interferon-induced transmembrane proteins. *Virology* **474**, 10–18 (2015).

41. Brahim Belhaouari, D. *et al.* The Strengths of Scanning Electron Microscopy in Deciphering SARS-CoV-2 Infectious Cycle. *Front Microbiol* **11**, 2014 (2020).

42. Hou, Y. J. *et al.* SARS-CoV-2 D614G variant exhibits efficient replication ex vivo and transmission in vivo. *Science (1979)* **370**, 1464–1468 (2020).

43. Shuai, H. *et al.* Attenuated replication and pathogenicity of SARS-CoV-2 B.1.1.529 Omicron. *Nature* **603**, 693–699 (2022).

44. Cameroni, E. *et al.* Broadly neutralizing antibodies overcome SARS-CoV-2 Omicron antigenic shift. *Nature* **602**, 664–670 (2022).

45. Mannar, D. *et al.* SARS-CoV-2 Omicron variant: Antibody evasion and cryo-EM structure of spike protein–ACE2 complex. *Science (1979)* **375**, 760–764 (2022).

46. Zhang, J. *et al.* Structural and functional impact by SARS-CoV-2 Omicron spike mutations. *Cell Rep* **39**, 110729 (2022).

47. Metzdorf, K. *et al.* TMPRSS2 Is Essential for SARS-CoV-2 Beta and Omicron Infection. *Viruses* **15**, 271 (2023).

48. Chin, A. W. H., Lai, A. M. Y., Peiris, M. & Man Poon, L. L. Increased Stability of SARS-CoV-2 Omicron Variant over Ancestral Strain. *Emerging Infectious Disease journal* **28**, 1515 (2022).

49. Hirose, R. *et al.* Differences in environmental stability among SARS-CoV-2 variants of concern: Both Omicron BA.1 and BA.2 have higher stability. *Clinical Microbiology and Infection* (2022) doi:https://doi.org/10.1016/j.cmi.2022.05.020.

Acknowledgements

Author Contributions

580   CMC, AWCY, WSB and ID conceived the study; JCB and KS generated the *in-vitro* data; CMC, AWCY and

581   ID conceived the mathematical models; CMC performed the analysis for Model 1; AWCY performed

582   the analysis for Model 2; CMC, AWCY, JCB, TPP, WSB, and ID contributed to the interpretation of the

583   results; CMC and AWCY wrote the first draft of the manuscript; all authors reviewed and approved the

584   final version of the manuscript.

Competing Interests

586   The authors declare no competing financial interests.

Data Availability

588   All data is available at https://github.com/ada-w-yan/deltaomicronmodelling

Code Availability

590   All code is available at https://github.com/ada-w-yan/deltaomicronmodelling

591